

Consequence of Nanometer-Scale Property Variations to Macroscopic Properties of CrOCN Thin Films

Jackson Smith,[†] Roger H. French,^{*,‡} Gerd Duscher,[§] and Dawn Bonnell^{*,†}

Department of Materials Science and Engineering, The University of Pennsylvania, Philadelphia, Pennsylvania 19104; Central Research, DuPont Company, Wilmington, Delaware 19880; and

Department of Materials Science, North Carolina State University, Raleigh, North Carolina 27695

Macroscopic properties of CrOCN thin films are related directly to composition and property variations on multiple length scales. Compositions resolved on a nanometer scale were measured in-depth in 120–150 nm thick CrOCN films by sputtered neutral mass spectroscopy. A statistical analysis of composition identifies the particular coordinations of the various anions with Cr that form preferentially under relevant processing conditions. Near-edge structure in electron energy loss from transmission electron microscopy and the Cr core level shift in X-ray photoemission spectroscopy further support this conclusion. A wide range of compositions are described in terms of mixtures of binary and ternary compounds, and optical absorption is found to be correlated with the presence of Cr⁴⁺ within this description. It appears that the presence of the unfilled t_{2g} state is responsible for optical absorption in the range of 0.5–6 eV and that a critical concentration of Cr⁴⁺ in certain species within the system is required for the transition to occur. These results conflict with the suggestion that a percolated network of metallic clusters is responsible for the change in properties.

I. Introduction

MANY advanced materials applications involve structure or composition variations on the nanometer length scale. Examples include semiconductor heterostructures, quantum dot arrays, and nanoclusters. Photomasks for optical lithography in semiconductor device manufacture are one such application which is of cutting edge technological interest. The latest photomask technology requires the precise control of properties such as optical transmission, reflectance, and chemical reactivity. A mask film composed of a series of nanometer-scale metal and oxide layers deposited on a transparent substrate will have resultant macroscopic optical properties that are a compromise between the extremes of metal and insulator optical properties. The composition and/or thickness of the various layers are varied to control the optical properties. For a given metal/oxide system, the number of possibilities for macroscopic optical constants scales inversely with the thickness of the metal/oxide layers. Therefore, a continuous gradation of composition from metal to oxide on an angstrom scale would allow the most

latitude in film optical properties. This has been previously demonstrated in the CrOCN system.^{1,2}

While tuning parameters in the deposition process to achieve desired macroscopic optical properties has produced successful commercial-grade CrOCN films, the contributions to macroscopic behavior of nanometer and atomic scale composition/property variations are not understood. The goal of the present study is to elucidate these contributions by determining the relationships between the optical and chemical properties on multiple length scales. In order to do this, coordinated measurements are taken of both optical and chemical properties with suitable spatial localization. A number of analytical tools are applied in order to make such correlations. The techniques employed extract compositional and optical information on the three length scales that define the problem: the 100–200 nm thickness of the composite film, the 10–20 nm widths over which deposition-controlled composition variations occur, and the ~1 nm atomic configurations ultimately responsible for all film properties. Sputtered neutral mass spectroscopy (SNMS) is used to determine composition on the nanometer scale as well as film thickness. Statistical modeling of composition variations is used to deduce atomic coordination. The electronic structure resulting from these coordinations is verified by spatially localized (nanometer scale) electron energy loss spectroscopy (EELS) in transmission electron microscopy (TEM) and by X-ray photoelectron spectroscopy (XPS). Macroscopic film optical properties as well as optical properties on the nanometer scale are extracted through variable-angle spectroscopic ellipsometry (VASE). The combination of results allows a description of properties based on behavior at all three length scales.

II. Experimental Procedure

The CrOCN thin films are deposited using reactive magnetron sputtering onto fused silica substrates. Cr targets are sputtered in the presence of N, O₂, CO₂, CH₄, and Ar at a total pressure on the order of 10⁻³ torr. The gas composition and cathode power are varied to produce the desired composition gradients in the film. The processing of these films is well documented³ and not within the scope of the present paper.⁴ Three CrOCN films in which composition gradients result in a 180° phase shift and controlled transmission of 248, 365, and 436 nm incident light are the subject of this study.³ The sample films are referred to by their operating wavelength (i.e., the film used to shift and attenuate 248 nm light is referred to as a “248 nm film”).

Composition profiles were determined by SNMS. Incident Kr atoms with an energy of 2 keV impacted samples at a glancing angle of 60° with respect to the surface normal. The incident beam was approximately 0.5 mm in width (the limit of spatial resolution) and yielded average sample sputtering rates of approximately 0.05 nm/s. The apparatus⁵ has a mass resolution of approximately 1 amu; 2 cm × 2 cm samples were sectioned from 12.5 cm × 12.5 cm plates and cleaned sequentially with liberal amounts of acetone and ethanol and subjected to ultrasonic cleaning.

J. J. Petrovic—contributing editor

Manuscript No. 188452. Received June 23, 2000; approved July 12, 2001.

This work was supported by the National Science Foundation, by the GAOLI Program, and by Central Research, DuPont Company. The facilities used were supported by the MRSEC program under Grant No. DMR 91-20668.

*Member, American Ceramic Society.

[†]University of Pennsylvania.

[‡]DuPont Company.

[§]North Carolina State University.

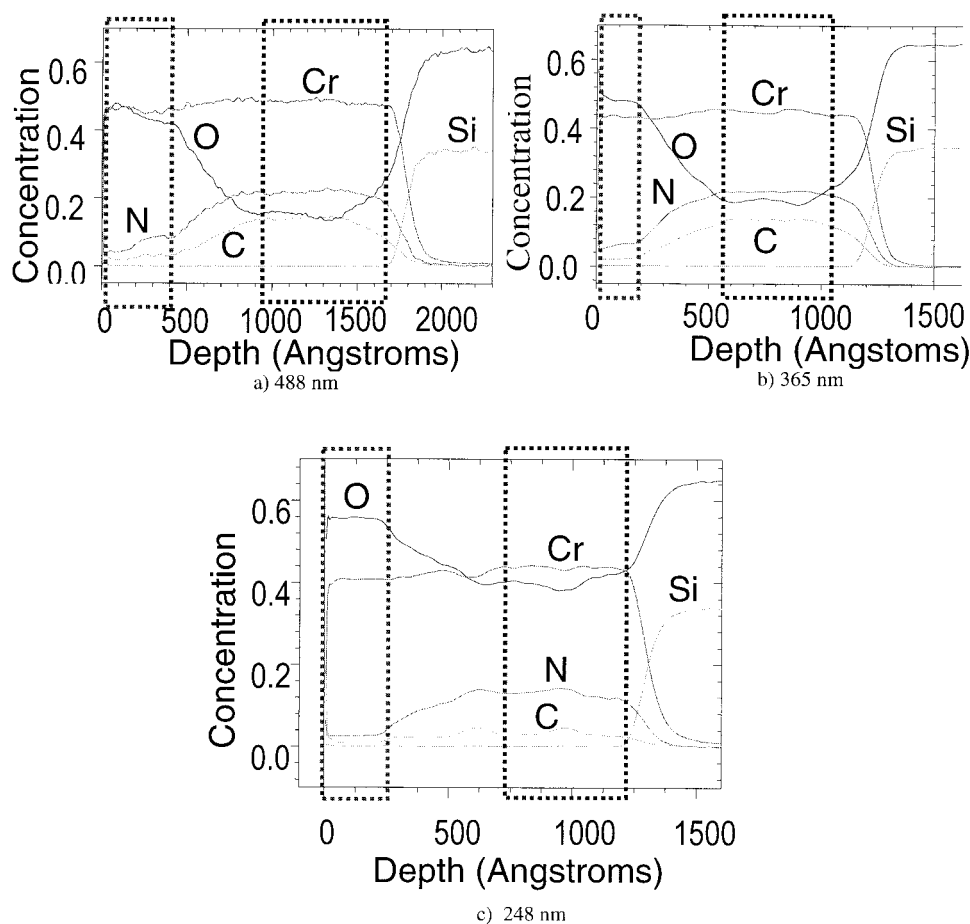
Two approaches were taken to relate changes in local bonding to composition. XPS sputter profiles were compared with EELS from scanning transmission electron microscopy (STEM). Both techniques provide information about local electronic structure with spatial resolution sufficiently small to be localized to the approximately 30 nm thick regions of constant composition at the top and bottom of the films. XPS was carried out in a PHI 600 ESCA lab system with a sputter rate of 20 Å/min. Since Auger electron spectroscopy and SNMS verified the presence of 2–5 nm of surface contamination, binding energies were not acquired before the carbon peak attained the bulk value. The Cr 2*p* binding energies are associated with the energies of the *p* orbitals and consequently are sensitive to local coordination. In general, sputtering data from oxide crystals can be ambiguous because the process often induces oxygen loss and reduction in these systems. However, Cr₂O₃ has been shown to be stable with respect to sputtering.⁶ EELS was carried out with a VG HB501 UX dedicated STEM equipped with a cold field emission source and parallel electron energy loss spectrometer (Gatan 666 PEELS). The beam current was in the range of 300 nA with a corresponding beam diameter of 1 nm, but sample charging caused some drift so the spatial resolution of the measurements is considered to be in the 3–4 nm range. TEM foils were made by gluing two films together, embedding them in alumina, sectioning them into 3 mm disks, dimpling and Ar ion milling.

Optical properties were measured with variable angle spectral ellipsometry (VASE) as described in detail in the Ref. 2. In VASE collimated and polarized monochromatic light beams of different wavelength are sequentially incident with various orientations with respect to the sample surface. Only front side ellipsometry was performed. This technique requires the back side of the quartz substrate to be mechanically roughened, to eliminate internal

reflection effects (due to the otherwise smooth and reflective surface). The reflected beams (one for each incident beam orientation or “angle”) are collected and their polarization is determined using a second polarizer. This allows the calculation of ρ , the ratio of the complex Fresnel reflection coefficients which can be used to determine the optical properties of the sample through computational modeling of the experiment. Again, 2 cm × 2 cm samples were sectioned from 12.5 cm × 12.5 cm plates and cleaned sequentially with liberal amounts of acetone and ethanol and subjected to ultrasonic cleaning. Ellipsometric data were then collected for each sample at glancing angles of 60°, 70°, and 80° for incident light beams with energies ranging from 1.5 to 6.6 eV in steps of 0.1 eV. The indices of refraction and extinction coefficients are determined from fitting an optical model⁷ of these films to these data. The model utilized information about physical features of the films (such as film thickness and the thickness and position of region of stable film chemistry) known from analysis of the SNMS results.

III. Results and Discussion

The composition profiles determined from SNMS are displayed in Fig. 1. Each profile contains varying proportions of Cr, O, N, and C throughout the film. The position of the substrate is indicated by the abrupt increase in the Si signal. The depth resolution of SNMS is 2 nm. Though film thickness varies, SNMS data confirm that each is in the range 120–300 nm. The SNMS



⁷J. A. Woolam's WVASE Data Acquisition and Analysis software for the PC used to model film.

Fig. 1. Composition profiles from sputtered neutrals mass spectroscopy showing composition gradients in the four CrOCN thin films. The regions outlined are defined as “nearly constant” compositions and 10–50 compositions within such a region are extracted for statistical analysis.

results also confirm the composition and illustrate how the gradient relates to parameters in the deposition process. Note that the "top" ~ 30 nm and the "bottom" ~ 30 – 50 nm regions (the boxed regions in the figure) are of relatively constant composition. Further, the "top" of each film is relatively high in oxygen content, while the film "bottoms" are relatively deficient in oxygen. The bottom region of each film also has a greater nitrogen content than the corresponding top region. There is a transition region that varies in thickness from 20 to 30 nm. The width of the "top" film region varies from ~ 20 nm for the 365 nm film to ~ 50 nm for the 488 nm film. Though the thickness of the transition region is similar for each film, there is considerable variation in the "bottom" layer. These thickness measurements are used in the determination of optical properties described below.

The compositions are related to atomic coordination with the statistical approach described in the Appendix. The results are compared to the bonding configurations found in binary chrome oxides. The bonding configuration of the film with $[O] = 0.56$ corresponds well to that of Cr_2O_3 ($a = 1.5$). As the analysis is unbiased in favor of this coordination, this result indicates that Cr_2O_3 is a major constituent in this film. In films with lower oxygen content, the coordination of the model binary oxide is less than 1.5. Consequently compounds with higher O to Cr coordinations such as occurs in CrO_2 and CrO_3 cannot be present unless accompanied by CrO . However, CrO is by far the rarest form of the chrome oxides. Further, XPS results on chromium oxide binary films made with the same process show no evidence of the existence of this compound, but clearly indicate the presence of Cr^{3+} (the valence state of Cr in Cr_2O_3 , see Ref. 7).

Another important result is that composition ratios for the binary nitrides in Table I cannot be explained in terms of combinations of stable binary compounds. This is best illustrated by example. If the composition with coordination $a = 1$, $b = 5.3$ (248 nm film bottom) is represented by binary compounds, then these must be of the form Cr_xO_x and $\text{Cr}_y\text{N}_{5.3y}$. In the simplest case, $x = y = 1$ and Cr must have a valence of $+2$ in coordination with oxygen and $+15.9$ in coordination with N, respectively. This is obviously unreasonable. Note that in all compositions the nitride is stoichiometric or metal deficient ($b \geq 1$) and the oxide is metal rich ($a \leq 1.5$). Therefore, if reasonable valence states of Cr hold, then the chemical basis set needs to be expanded beyond the chrome binary restriction in Eq. (A-1).

The compositions can be accounted for by adding a $\text{Cr}_x\text{O}_y\text{N}_z$ ternary compound to the description. Note that the analysis of the composition data in terms of binary compounds clearly indicates the presence of Cr_2O_3 at compositions with high $[O]$ (Table I), which is confirmed by XPS reported elsewhere.⁸ Therefore, Cr_2O_3 is a major constituent in these films. Also, Cr bonds octahedrally to anions in all stable compounds. Consequently, Cr-anion bonding can be expected to be octahedral in these materials. Further, both the O^{2-} and N^{3-} ions have similar valence and similar size (ionic radii of 1.3 and 1.7 Å, respectively). These observations suggest that the ternary compound can be viewed as Cr_2O_3 with substantial N substitution for O. The presence of a $\text{Cr}_2\text{O}_x\text{N}_{(3-x)}$ bonding configuration is also consistent with the property variation since N substitution for O will alter the local electronic structure.

In the spirit of Zacharisen's description of simple oxide glasses, CrOCN amorphous compounds are described as linked polyhedra. In all except a couple of very unstable complexes Cr is octahedrally coordinated in crystalline compounds and in organic and inorganic complexes. Therefore, the description employed maintains that each Cr atom has an octahedral coordination in these films. In $\text{Cr}^{\text{III}}\text{O}_3$ the O is tetrahedrally coordinated, and in $\text{Cr}^{\text{IV}}\text{O}_2$ it is trigonally coordinated. Balancing electrostatic bond strength with anion charge⁹ in $\text{Cr}_2^{\text{III}}\text{O}_3$ around the octahedron shown in Fig. 2(a) gives an oxygen coordination of 4. If one O were replaced by N producing $\text{Cr}_2\text{O}_2\text{N}$, Fig. 2(b), the coordinations of both O and N would be 4. In this case the Cr oxidation state is 3.5, which indicates disproportionation into Cr^{3+} and Cr^{4+} . Replacing two of the O by N to form $\text{Cr}_2^{\text{IV}}\text{ON}_2$ gives the octahedron shown in Fig. 2(c) and the electrostatic bond strength calculation yields tetrahedrally coordinated O and trigonally coordinated N with Cr in the 4+ oxidation state. The anion coordinations can be satisfied by a combination of edge and corner sharing in a structure that exhibits no long-range order.

These bonding configurations should be manifest in the electronic structure of the films as measured by EELS and STEM. Figure 3 shows a dark-field TEM image of the cross section of an optical film. Photoemission spectra were acquired at sputter times that correspond to the positions numbered 2 and 4, the bottom and top of the film, respectively. Figure 4 shows the Cr 2*p* binding energies; the 2*p*_{3/2} peak occurs approximately 1.25 eV lower for the bottom film region than it does for the surface. The bottom region has anion/cation coordinations of $a = 0.50$ and $b = 2.58$, while at the top of the film $a = 1.33$ and $b = 1.01$. That the higher N coordination produces a lower Cr 2*p* binding energy is consistent with a local coordination change causing a change in Cr valence. Compare the energies in Fig. 4 with those for 2*p*_{3/2} binding energies for Cr metal, CrIVO_2 , and $\text{Cr}^{\text{III}}\text{O}_3$, which are 574.4, 576.1, and 576.6 eV, respectively.¹⁰ If, instead, discrete CrN or Cr metal were present, the peak would broaden and eventually develop a shoulder centered at 575 eV.¹¹

A comparison of the energy loss at the O *K* edge measured in STEM at positions 1 and 5 is shown in Fig. 5(a) for a similar film. As is usual with transition-metal oxides the O *K* edge, which is associated with a 1*s*-to-2*p* transition, has two distinct peaks.^{12,13} The initial peak at 531 eV and one centered at about 542 eV are ascribed to hybridization of O 2*p* with empty Cr 3*d* orbitals. The broad peak above 560 eV is related to O 2*p* metal, 4*sp* hybridization.¹⁴ The data in Fig. 5(a) have not been corrected for multiple scattering or thickness variation, so while relative peak energies can be compared, peak intensities cannot. No shift in the O *K* edge occurs to within the accuracy of the measurement. The primary difference between the low (top) and high (bottom) N content regions is peak broadening in the former and an additional peak in the latter. It can be speculated that the broadening is associated with a dispersion in O–O bond lengths.

Comparison of the Cr *L*₂, *L*₃ edges yields a more quantitative result. The spectra shown in Fig. 5(b) are corrected for multiple scattering. Both the O contribution to the Cr edge and the free electron continuum were subtracted. The procedure is discussed in detail in Refs. 15–18. The resulting white lines are associated with

Table I. Results of Statistical Analysis

Film operating wavelength (nm)	Film thickness (Å)	Film region	[O]	[N]	[C]	[Cr]	<i>a</i>	<i>b</i>	<i>c</i>
coq [†]	1029	Top	0.32	0.19	0.06	0.43	0.82 ± 0.15	5.64 ± 1.00	9.91 ± 1.02
		Bottom	0.01	0.23	0.05	0.71	0.02 ± 0.05	1.12 ± 0.53	9.30 ± 0.43
436	1257	Top	0.44	0.07	0.03	0.46	1.02 ± 0.05	2.74 ± 0.31	9.85 ± 0.36
		Bottom	0.15	0.22	0.14	0.49	0.37 ± 0.15	3.12 ± 0.18	9.90 ± 0.25
365	1082	Top	0.48	0.06	0.02	0.43	1.17 ± 0.05	3.39 ± 0.09	9.89 ± 0.22
		Bottom	0.19	0.22	0.14	0.45	0.47 ± 0.05	6.93 ± 0.24	9.99 ± 0.29
248	1109	Top	0.56	0.03	0.01	0.41	1.42 ± 0.05	2.05 ± 0.12	9.97 ± 0.04
		Bottom	0.40	0.13	0.03	0.44	0.97 ± 0.05	5.28 ± 0.26	9.98 ± 0.34

[†]Chrome on quartz.

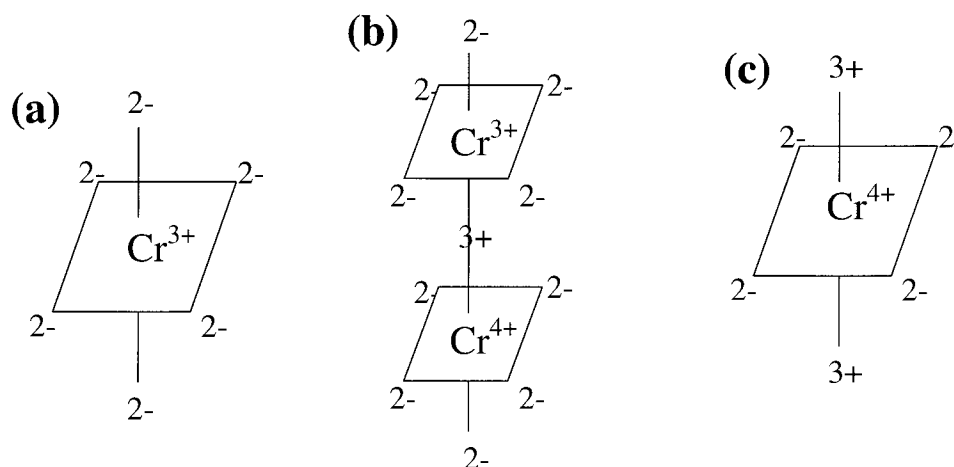


Fig. 2. Coordination polyhedra for Cr_2O_3 and CrO_2 (a), $\text{Cr}_2\text{O}_2\text{N}$ (b), and Cr_2ON_2 (c) illustrating the geometric arrangements of N substitution. Numbers in figure represent the formal charge of anions.

the density of states of the empty d bands. The relative differences in the peak intensity ratios ($L3/L2$) and the sum of these intensities to that of the background ($(L2 + L3)/\text{continuum}$) are well outside any error in background subtraction procedures. The $L3/L2$ ratio increases with electron occupancy of d orbitals, while the white line/continuum ratio decreases with electron occupancy.¹⁹ The data are summarized as follows:

For $a = 0.50$ and $b = 2.58$, $L3/L2 = 2$, and $(L2 + L3)/\text{continuum} = 1$.

For $a = 1.33$ and $b = 1.01$, $L3/L2 = 3$, and $(L2 + L3)/\text{continuum} = 0.5$.

The oxygen-rich composition ($a = 1.33$) has larger $L3/L2$ and lower $(L2 + L3)/\text{continuum}$, indicative of higher electron occu-

pancy of d orbitals. This is again consistent with N replacement of O in Cr coordination.

The relation of local composition to local optical properties is determined using the data discussed above and ellipsometric measurements. Figures 6 and 7 compare the concentration and anion:cation dependencies of extinction coefficient (k) determined from optical models of ellipsometry data. The extinction coefficient is proportional to the optical absorption, α , for a particular wave length of incident radiation ($\alpha = 2\pi k/\lambda$). As expected, there is a decrease in k at 3.4 eV with increasing oxygen content and concomitant decreasing nitrogen content. There is not a good correlation with Cr content, in that of the three compositions with >45% Cr only two exhibit large

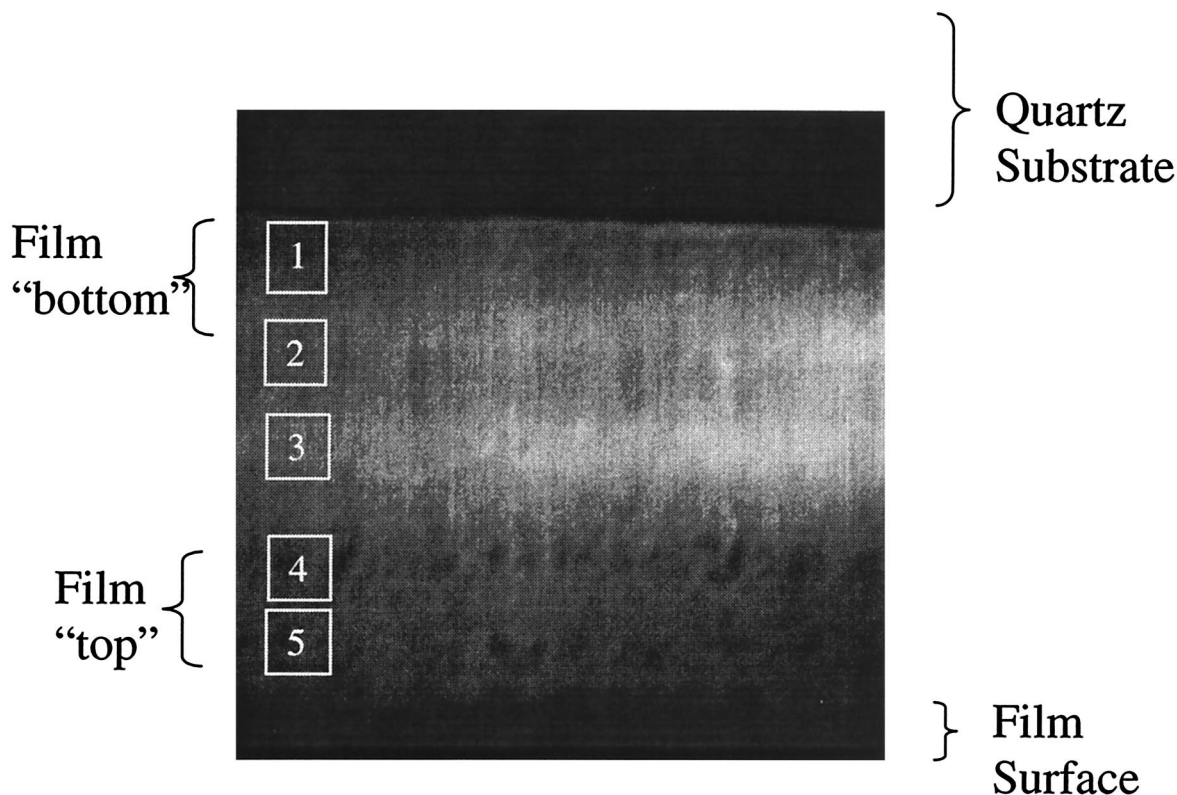


Fig. 3. Bright-field image of a CrOCN thin film indicating where XPS and spatially resolved EELS were obtained.

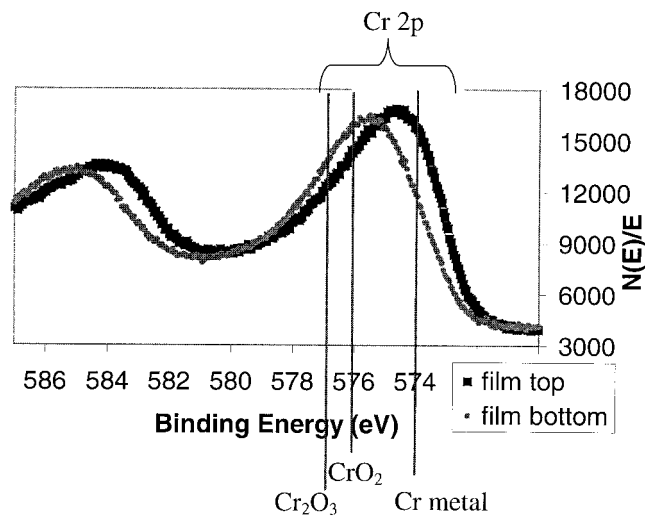


Fig. 4. XPS spectra of a CrOCN thin film comparing the Cr 2p core level shift associated with N substitution with the 2p binding energy in binary compounds. The dotted curve is for the composition where the anion coordinations were $a = 0.5$, $b = 2.58$ and the solid curve is where the anion coordinations were $a = 1.33$, $b = 0.101$.

extinction coefficients. However, it can be seen from Fig. 7 that those compositions with an O:Cr ratio of 0.5 and nitrogen ratio $2 < \text{N:Cr} < 3$ have extinction coefficients 2 to 3 times higher than all other compositions. The fact that compositions with N:Cr ratios above and below this range exhibit low absorption

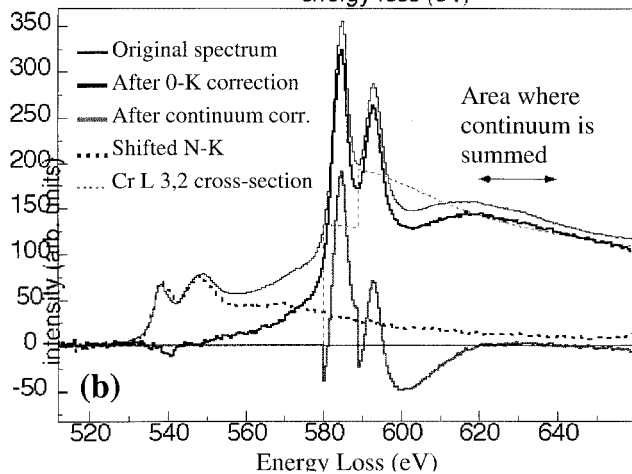
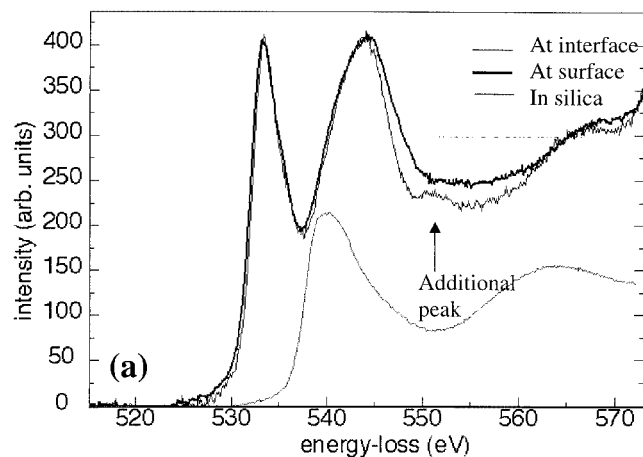


Fig. 5. EELS spectra for a CrOCN thin film. The anion coordinations were $a = 0.5$, $b = 2.58$ for top and $a = 1.33$, $b = 0.101$ for film bottom: (a) raw spectrum, (b) scattering corrected spectrum.

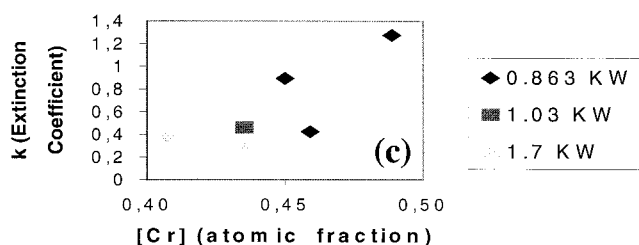
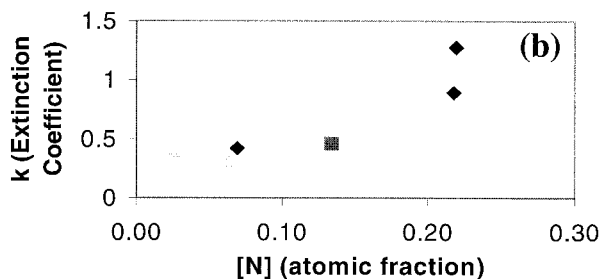
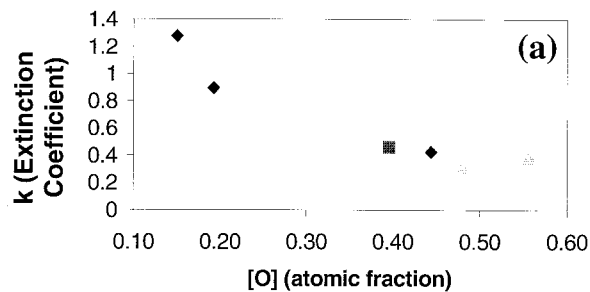


Fig. 6. Composition dependence of extinction coefficient at 3.4 eV determined from a combination of optical and compositional analyses results for [O] in (a), [N] in (b), and [Cr] in (c). (Each point represents 10–50 composition measurements.)

suggests that b is not an independent parameter. By comparing Fig. 7 with Table II, it is clear that as the amount of Cr^{3+} in the ternary compound decreases from 100% to 50% there is no significant difference in the extinction coefficient. Large absorption does occur, however, when all of the Cr in the complex is in the 4+ state. This is consistent with the fact that +4 Cr in crystalline solids, exemplified by CrO_2 , are metallic.

In the ligand field description of octahedral coordination of transition metals the d orbitals split into three lower lying degenerate t_{2g} orbitals, and two upper lying degenerate e_g orbitals, as illustrated in the schematic molecular orbital diagram of Fig. 8. If Cr has a formal charge of 3+, the three lower orbitals are filled with one electron each, leaving a gap to the unoccupied e_g orbitals. For Cr^{4+} only two of the t_{2g} orbitals contain electrons; the third is no longer degenerate and must be at a higher energy (Fig. 8). There is some discrepancy between spin resolved photoemission results and band structure calculations as to whether the widths of the bands resulting from these d orbitals are sufficiently wide for overlap at the Fermi energy leading to conductivity, or whether there is a completely unoccupied gap between them. Recent calculations suggest that spin coupling leads to hybridization of the distorted orbitals allowing a finite density of states at the Fermi energy.²⁰ Ultraviolet photoemission spectroscopy²¹ indicates that for $\text{Cr}^{\text{IV}}\text{O}_2$ the top of the O 2p orbital is 2–2.5 eV below the top of the filled t_{2g} . The filled t_{2g} is 1.6 eV wide and is 2.2 eV from the unoccupied t_{2g} in agreement with earlier optical studies¹² to within 10% in energy. Replacing some of the oxygen by nitrogen will further distort the crystal field. For the compound depicted in Fig. 2(c) two oxygen atoms remain at opposite apices of the octahedron to maximize the distance between

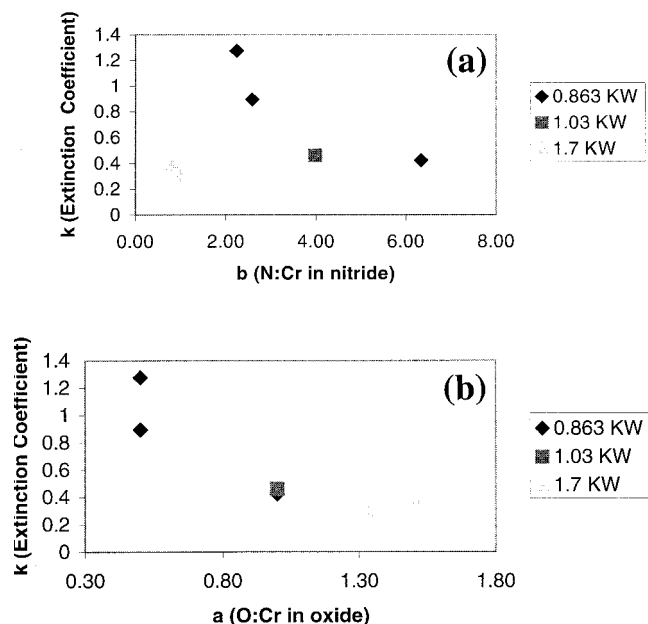


Fig. 7. Effect of anion:cation coordination on optical absorption. Extinction coefficient dependence on O:Cr (a) and N:Cr (b). (Each point represents 10–50 composition measurements.)

them. The field strength will be larger and distortion will occur along the z -axis, thereby eliminating the energy difference of the orbitals. This is illustrated in Fig. 8. An O $2p$ to unfilled t_{2g} transition would have an energy in the range 3.1 to 4.7 eV for the Cr^{4+} octahedra and that of the Cr_2O_3 bandgap, 4.8 eV, for Cr^{3+} when coordinated with O. The O $2p$ to t_{2g} transition in the ternary compound will occur at a somewhat higher energy if the field distortion separates the p and d orbitals. These transitions are expected to dominate the optical properties of these materials since free carrier absorption and transitions between d orbitals (allowed because the symmetry is broken) will be ≤ 1 eV¹² and have lower intensity. The preceding discussion could have been equally well carried out in the context of band theory instead of crystal field theory, leading to the same conclusions.

Figure 9 shows the spectrally resolved optical constants for the top and bottom regions of each film obtained by modeling the ellipsometry data. A sharp absorption peak occurs around 5.00, 4.75, and 5.5 eV in the spectra of the bottom material for the 488, 365, and 248 nm films, respectively. The background absorption and peak edges are not as sharp as in crystalline solids because the films are amorphous. The bottom regions of each film have O:Cr coordinations of 1.00 or less and therefore contain the least amount of Cr(III) (see Fig. 2). The edge of this absorption peak is less sharp and occurs at higher energies for the film top regions, 6.5, 5.75, and 6.1 eV. Several of these compositions also exhibit evidence of shoulders around 4 eV. These regions have higher O:Cr coordinations than the film bottoms and so contain more Cr(III). Since the sharpest 5 eV absorption edge appears to occur in portions of the films that contain Cr_2ON_2 and the energy is in the correct range, it appears that this absorption represents the O $2p$ to unfilled t_{2g} transition. The shift toward higher energy with increasing oxygen could be a contribution of the Cr^{3+} octahedra. Therefore, the details of the optical spectra, as well as the compositional analysis, support the view that anion substitution can be used to systematically control the optical absorption.

The reasons for neglecting CrN and CrC binary compounds in this discussion are as follows. While chromium also adopts a formal 3+ valence in CrN and has a finite density of states at the Fermi level, the measured absorption does not correlate with the presence or content of CrN. If present, the amount of CrN is sufficiently low to prevent the realization of the metallic electronic

structure of the compound in the films. This is consistent with our composition data in that there would be very little of the N left for forming CrN if 50% or more of it were consumed in a ternary compound. The argument for CrC binary compounds is similar in that film optical properties are unrelated to [C]. There is, however, carbon excess in the binary compounds that best describe all compositions. This leads to our hypothesis of the presence of a Cr-doped C impurity. Since the bonding of C varies from metallic to insulating, the C contribution to the optical properties cannot realistically be accessed; however, as the amount of C is usually less than 5 at.%, its presence should not dominate properties.

IV. Conclusions

A statistical approach to composition analysis has identified anion:cation ratios that occur in reactive sputtered CrOCN thin films. A wide range of overall compositions is achieved through the formation of ternary compounds in combination with binary compounds. A correlation of optical absorption was found for O:Cr and N:Cr ratios. Evidence for the relation of optical properties to the ternary compound comes from the energy of peaks in optical absorption, the Cr $2p$ core level shift in XPS, and $L3/L2$ white line ratios in EELS. An optical absorption at about 5 eV is most sharp when the amount of Cr associated with O containing binary or ternary compounds of our description goes to 0. In particular it appears that the presence of the unfilled t_{2g} state is responsible for optical absorption and that a critical concentration above 50% is required. The evidence is incompatible with a percolated network of metallic clusters that is responsible for the change in properties.

The determination of parameters at all three length scales (100–200 nm film thickness, 10–20 nm composition variation and atomic coordination) have been linked in a comprehensive explanation of film chemical and optical properties. Implications here are general and the approach can be used to develop new combinations of chemistry and geometries for arbitrary requirements in optical properties.

Appendix

Analytical Approach

The goal of the statistical analysis of the composition variation in the films is to determine the preference for specific coordination with Cr. Film composition at any point is described according to the following relation:

$$\text{Composition} = X\text{CrO}_a + Y\text{CrN}_b + Z\text{CrC}_c \quad (\text{A-1})$$

where a , b , and c represent the anion coordination to Cr and X , Y , and Z the relative amount of binary oxide, nitride, and carbide, respectively. Since all compositions contain excess anions, it might be assumed that metallic Cr does not exist in the films. It will be shown in later sections, however, that the presence of chrome metal is likely in certain compositions. These results also show that C is present as an impurity in that [C] shows no detectable affect on film properties and the amount of this species in most compositions of CrOCN is small relative to the other species. Then, the binary chrome carbide species in Eq. (A-1) can be considered to account for any metallic chrome in the system.

Some useful relationships between these variables and quantities obtained from SNMS data include the following:

$$[\text{O}] = X \cdot a$$

$$[\text{N}] = Y \cdot b$$

$$[\text{C}] = Z \cdot c$$

$$[\text{Cr}] = X + Y + Z$$

where brackets indicate the concentration in atomic fraction.

Table II. Compound Formation in CrOCN Films

% of Cr(III) in Cr _x O _y N _z	<i>a</i>	<i>b</i>	<i>c</i>	Compounds [†]
0	0.5	2.5	5.0	$\frac{3}{4}(\text{Cr}_2^{\text{IV}}\text{ON}_2) + \text{Cr}^{\text{III}}\text{N} + \text{CrC} + \text{carbon impurity}$
50	1.0	4.0	9.0	$1.5(\text{Cr}_2^{\text{IV}}\text{ON}_2 + \text{Cr}_2^{\text{III}}\text{O}_3) + \text{Cr}^{\text{III}}\text{N} + \text{CrC} + \text{carbon impurity}$
50	1.0	6.0	9.0	$2.5(\text{Cr}_2^{\text{IV}}\text{ON}_2 + \text{Cr}_2^{\text{III}}\text{O}_3) + \text{Cr}^{\text{III}}\text{N} + \text{CrC} + \text{carbon impurity}$
83	1.33	2.0	9.0	$(\text{Cr}_2^{\text{IV}}\text{ON}_2 + 5\text{Cr}_2^{\text{III}}\text{O}_3) + 2\text{Cr}^{\text{III}}\text{N} + \text{carbon impurity CrC}$
100	1.5	1.0	5.0	$\text{Cr}_2^{\text{IV}}\text{ON}_2 + \text{Cr}^{\text{III}}\text{N} + \text{CrC} + \text{carbon impurity}$
0	0.5	2.5	5.0	$\frac{3}{4}(\text{Cr}_2\text{ON}_2) + \text{Cr}^{\text{III}}\text{N} + \text{CrC} + \text{carbon impurity}$
50	1.0	4.0	9.0	$3 \text{Cr}_2^{\text{III,IV}}\text{O}_2\text{N} + \text{Cr}^{\text{III}}\text{N} + \text{CrC} + \text{carbon impurity}$
50	1.0	6.0	9.0	$5 \text{Cr}_2^{\text{III,IV}}\text{O}_2\text{N} + \text{Cr}^{\text{III}}\text{N} + \text{CrC} + \text{carbon impurity}$
83	1.33	2.0	9.0	$\text{Cr}_2^{\text{III,IV}}\text{O}_2\text{N} + 2\text{Cr}_2\text{O}_3 + \text{Cr}^{\text{III}}\text{N} + \text{CrC} + \text{carbon impurity}$
100	1.5	1.0	5.0	$\text{Cr}_2\text{O}_3 + \text{Cr}^{\text{III}}\text{N} + \text{CrC} + \text{carbon impurity}$

[†]The valence of Cr is indicated by superscripts in each compound; i.e., CrO becomes Cr^{II}O.

It is assumed that oxygen has first preference in satisfying bonding with Cr when all three anions are present. Earlier studies⁵ of reactive magnetron sputtering of films with binary (CrX₂, where X = O, N, or C) compositions showed empirically that of the anions in this study O has the highest reactivity with Cr (see Ref. 22). Cr was completely oxidized with a minimal amount of O in the reaction stream, whereas higher concentrations of C or N were required to form nitrides and carbides. This result is consistent with the fact that the binding energies of the chrome oxides are much higher than those for chrome carbides and nitrides. In the statistical analysis, the O:Cr coordination *a* is allowed to take on all values between 0.01 and 10 that are integer multiples of 0.01. These values are chosen so that coordinations corresponding to the common chromium oxides are included, as well as some that do not exist in nature. Encompassing unexpected oxide coordinations is deliberate; it allows our model to test the assumption that local bonding in the films approximates the bonding in crystalline solids. The N:Cr and C:Cr ratios are allowed to vary continuously between 0.01 and 10 in order to encompass all anion:Cr coordinations for binary carbides and nitrides.

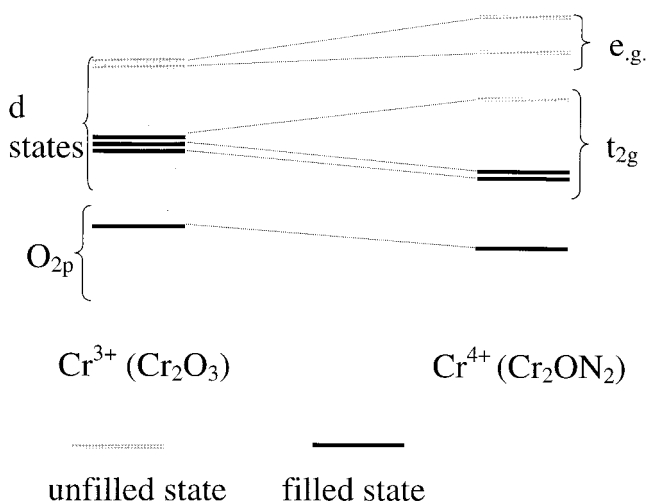


Fig. 8. Schematic diagrams of orbitals for a transition-metal cation in an octahedral field as in Cr₂O₃ and the trends in energy variation with change in Cr valence as in CrO₂ and with change in anion coordination as in Cr₂ON₂ as shown.

Local composition is extracted from the SNMS profile in the regions of relatively stable composition. Each region is represented by a data set, which includes 10–50 composition measurements. For example, composition measurements in the surface left box in Fig. 1(a) are used to characterize the deposition under the conditions necessary to make that particular layer (0.85 kW and 7, 24, and 3.75 sccm for O₂, N₂, and CH₄ flow rates, respectively). For each composition measurement in a set, *b* and *c* are adjusted continuously for each of the O:Cr ratios, *a*, in order to minimize the fit parameter:

$$\{([\text{O}]_{\text{measured}} - [\text{O}]_{\text{calculated}})^2\}^{1/2} = \left\{ \left[[\text{O}]_{\text{measured}} - a \left(\frac{[\text{Cr}]_{\text{measured}}}{b} - \frac{[\text{C}]_{\text{measured}}}{c} \right) \right]^2 \right\}^{1/2}$$

Statistical analysis of the results of fitting all points yields a best fit *a*, *b*, and *c* for the data set. The oxygen coordination that is the best fit for the majority of the data points is then considered the best fit ‘*a*’ for the data set. The best fit ‘*b*’ and ‘*c*’, nitrogen and carbon coordinations, respectively, are the averages of those corresponding to the best fit oxygen coordination. The standard deviation of each fit coordination distribution provides a measure of the total error of this process, including the experimental error in the SNMS data and the actual composition variation within the relatively stable composition region that each data set represents.

$$\{([\text{O}]_{\text{measured}} - [\text{O}]_{\text{calculated}})^2\}^{1/2} = \left\{ \left[[\text{O}]_{\text{measured}} - a \left(\frac{[\text{Cr}]_{\text{measured}}}{b} - \frac{[\text{C}]_{\text{measured}}}{c} \right) \right]^2 \right\}^{1/2}$$

Statistical analysis of the results of fitting all points yields a best fit *a*, *b*, and *c* for the data set. The oxygen coordination that is the best fit for the majority of the data points is then considered the best fit *a* for the data set. The best fit *b* and *c*, nitrogen and carbon coordinations, respectively, are the averages of those corresponding to the best fit oxygen coordination. The standard deviation of each fit coordination distribution provides a measure of the total error of this process, including the experimental error in the SNMS data and the actual composition variation within the relatively stable composition region that each data set represents.

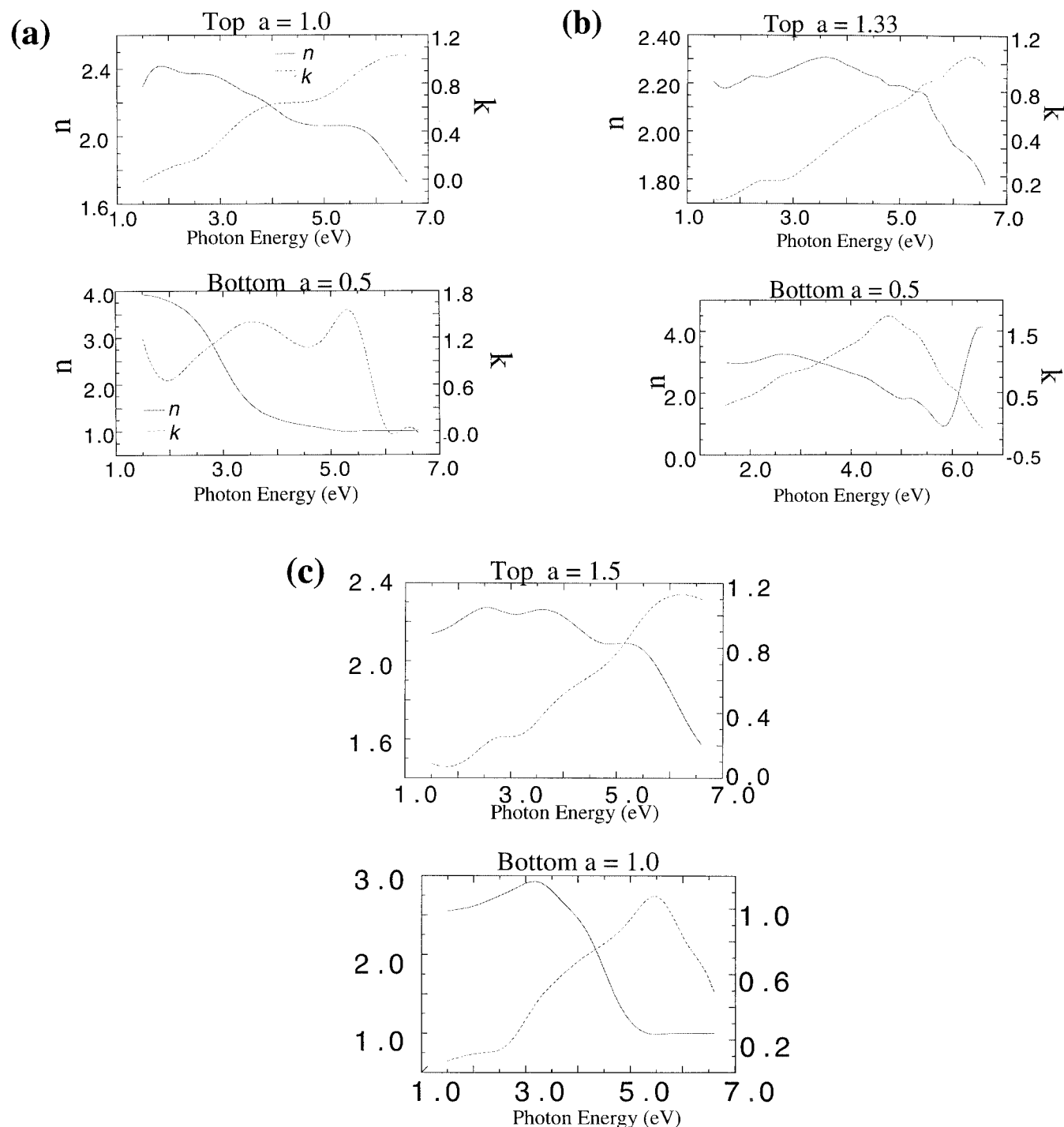


Fig. 9. Spectrally resolved optical constants that are spatially localized to 100–500 nm in CrOCN thin films. As labeled in (a), the dotted curves represent the extinction coefficient k and the solid the index of refraction n : (a) 488 nm film, (b) 365 nm film, (c) 248 nm film.

Acknowledgments

We appreciate help with the XPS from Dr. P. Graat and with the TEM sample preparation from U. Salzberg. We also acknowledge the general support of M. Rühle and from the Max Planck Institut fuer Metallforschung.

References

- ¹F. Kalk, R. H. French, H. Alpay, and G. Hughes, "Cr Based Attenuated Embedded Shifter Preproduction," *SPIE Proc.*, **2322**, 299–304 (1994).
- ²B. Johs, R. H. French, F. D. Kalk, W. A. McGahan, and J. A. Woollam, "Optical Analysis of Complex Multilayer Structures Using Multiple Data Types," *SPIE Proc.*, **2253**, 1098–106 (1994).
- ³H. Alpay, R. French, and R. Kalk, U.S. Pat. No. 5 415 953, 1995.
- ⁴F. Kalk, R. French, H. Alpay, and G. Hughes, "Attenuated Phase Shifting Photomasks Fabricated from Cr-Based Embedded Shifter Blanks," *SPIE Proc.*, **2254**, 64–70 (1994).
- ⁵Built in house by Dennis Schwartzfeger of DuPont Central Research and Development.
- ⁶V. Di Castro, C. Frulani, G. Polzonetti, and C. Cozza, "AES and Photoemission Studies of Cu Growth on Cr₂O₃," *J. Electron. Spectrosc.*, **46**, 297–302 (1988).
- ⁷R. H. French, D. J. Jones, F. D. Kalk, C. M. Wilson, and H. U. Alpay, "Phase Shifting Mask Photobank with Attenuating Film Absorber—SEMATECH Milestone 2, DuPont Progress Report 1994-CRD-289.
- ⁸J. R. Smith, P. C. J. Graat, D. A. Bonnell, and R. H. French, "Relation Between Local Composition, Chemical Environment and Phase Shift Behavior in Cr-Based Oxycarbonitride Thin Films," *Proc. Mater. Res. Soc.*, in press.
- ⁹A. R. West, *Introduction to Solid State Chemistry*. Wiley, New York, 1984.
- ¹⁰Handbook of XPS PHI.

¹¹G. Gewinner, J. C. Peruchetti, A. Jaegle, and A. Kalt, "Photoemission Study of the Chromium(111) Surface Interacting with Oxygen," *Surf. Sci.*, **78**, 439–58 (1978).

¹²C. Ortiz, T. Manoubi, and C. Colliex, "Physical Properties of Thin Films of Iron Oxides," *J. Phys. (Paris)*, 2009–10 (1988).

¹³P. N. Rowley, R. Brydson, J. Little, S. R. J. Saunders, H. Sauer, and W. Engel, "The Effects of Boron Additions on the Oxidation of Fe–Cr Alloys in High-Temperature Steam: Analytical Results and Mechanisms," *Oxid. Met.*, **35**, 375–95 (1991).

¹⁴F. M. F. de Groot, M. Grioni, and J. C. Fuggle, *Phys. Rev. B*, **40** [8] 5715–23 (1989).

¹⁵T. G. Sparrow, B. G. Williams, C. N. R. Rao, and J. M. Thomas, "White Line Intensity Ratio in Electron Energy-Loss Spectra of 3d Transition Metals," *Chem. Phys. Lett.*, 547–50 (1984).

¹⁶H. Kurata and C. Colliex, "Electron Energy-Loss Core-Edge Structures in Manganese Oxides," *Phys. Rev. B*, **48**, 2102–108 (1993).

¹⁷S. Suzuki and M. Tomita, "Valence Dependence of Electron Energy Loss Spectra of Chromium Oxides," *Jpn. J. Appl. Phys.*, **36**, 4341–45 (1997).

¹⁸D. H. Pearson, B. Fultz, and C. C. Ahn, "Measurements of 3d State Occupancy in Transition Metals Using Electron Energy Loss Spectroscopy," *Appl. Phys. Lett.*, **53** [15] 1405–407 (1998).

¹⁹R. F. Egerton, *Electron Energy-Loss Spectroscopy in the Electron Microscope*, 2nd ed. Plenum Press, New York, 1986.

²⁰M. Korotin, V. Anisimov, D. Khomiskii, and G. Sawatsky, "CrO₂: A Self-Doped Double Exchange Ferromagnet," *Phys. Rev. Lett.*, **80**, 4305–308 (1998).

²¹K. Kamper, W. Schmitt, G. Gunterodt, R. Gambino, and R. Ruf, "CrO₂—A New Half Metallic Ferromagnet?," *Phys. Rev. Lett.*, **39**, 2788–91 (1987).

²²M. Wagner, J. Smith, D. Bonnell, R. H. French, P. F. Carcia, unpublished work. □